ESD-TDR-64-36

Group Report

1964-14

S. L. Borison

Electromagnetic Backscattering Cross Section of a Circular Cylindrical Section

18 February 1964

Prepared for the Advanced Research Projects Agency
under Electronic Systems Division Contract AF 19(628)-500 by

Lincoln Laboratory
MASSACHUSETTS INSTITUTE OF TECHNOLOGY
Lexington, Massachusetts

The work reported in this document was performed at Lincoln Laboratory, a center for research operated by Massachusetts Institute of Technology. This research is a part of Project DEFENDER, which is sponsored by the U.S. Advanced Research Projects Agency of the Department of Defense; it is supported by ARPA under Air Force Contract AF 19(628)-500 (ARPA Order 498).

MASSACHUSETTS INSTITUTE OF TECHNOLOGY

LINCOLN LABORATORY

ELECTROMAGNETIC BACKSCATTERING CROSS SECTION OF A CIRCULAR CYLINDRICAL SECTION

S. L. BORISON

Group 41

GROUP REPORT 1964-14

18 FEBRUARY 1964

LEXINGTON MASSACHUSETTS

Electromagnetic Backscattering Cross Section of a Circular Cylindrical Section

Abstract

The electromagnetic backscattering cross section of a perfectly conducting circular cylindrical section is expressed in the Kirchoff approximation. The cross section for incidence at an arbitrary angle in either a longitudinal or a transverse plane is related to a geometrical structure integral. Using methods of contour deformation, this integral is approximated for the case of large linear dimensions compared to the incident wavelength. Comparison of the cross section with that of the equivalent flat plate (equal aperture) indicates that the central lobe of the flat plate is reduced by the factor $1/8\ (R/\lambda)\ \sin^2 \psi_m$; however, the angular width in the transverse plane is increased to approximately $2\psi_m$. (R = radius of curvature; ψ_m = aperture half-angle.) Typical values of R and ψ_m are chosen for calculation and the results are presented pictorially.

This technical documentary report is approved for distribution.

Franklin C. Hudson, Deputy Chief
Air Force Lincoln Laboratory Office

I. Introduction

The reflection of electromagnetic waves from a circular cylindrical section is often approximated by one of two extremes. If the section is of small depth compared to a wavelength, it seems intuitive to use the equivalent aperture flat plate. The reflection properties of large flat plates (dimensions large compared to a wavelength) have been studied by many authors, and it is well known that the Kirchoff approximation yields good results for the backscattered cross section.[1],[6]

If the cylindrical section is of large depth, geometrical optics implies that only a small region near the specular point will be important. One then finds a constant amplitude confined to the specular region of incidence. Since there are no backscattering specular angles for a cylinder when the incident direction is not in a transverse plane, one suspects this is generally a poor approximation. Marcus[2] treated this case for the general curved surface; however, his techniques do not allow one to define a cross section for the finite cylinder. More sophisticated techniques are usually applied to the open cylinder which is semi-infinite. The open, finite cylinder was treated by Keller[3] but the results only apply to dielectric materials with low conductivity. In a later paper, Keller[4] applied his geometric theory of diffraction to the finite cylindrical section, but the results for reflection correspond to geometrical optics. Steinberg and Wolf[5] begin with a general technique for the arbitrary cylinder, but their results evaluated to lowest order again correspond to geometrical optics for a closed cylinder. One might use the results obtained for a closed cylinder which approximates the one of interest in the region of illumination; however, for angles of incidence which possess specular regions near the edge of the open cylinder, this will again be a poor approximation.

The interesting case for a cylindrical section with depth of the order of

one wavelength does not seem to fit either of these investigated extremes. In particular, one would like to know how the lobe structure will differ from that of the equivalent flat plate, especially near the large central lobe specular region. Furthermore, for a small but finite aperture angle, there exist interesting regions of incidence for which there is no backscattering specular reflection.

In order to obtain some information about the lobe structure and the magnitude of the cross section in regions of no specular contributions, the Kirchoff approximation has been assumed for the surface current density. In Section II, the scattered field and backscattering cross section are formulated. Section III lists for comparison the well-known results of the Kirchoff approximation for large flat plates. In Section IV the scattered field is evaluated for two cases: 1) the longitudinal case for which the incident wave vector has no component orthogonal to the central element, 2) the transverse case for which the incident wave vector is orthogonal to any element. In both cases the scattered field depends on the evaluation of a structure integral. It is shown that the limiting case of the flat plate is contained in this function by a series expansion for small aperture angle (see Appendix B); however, for the case of large aperture depth this expansion does not converge. The structure integral is then evaluated by keeping the asymptotic results found by deforming the integration contour to one of stationary phase.

The results obtained by using these fields to calculate the backscattered cross section indicate two significant results. One finds that the peak value of the equivalent flat plate central lobe is reduced by a factor $1/8(R/\lambda)\sin^2\psi_m$. Furthermore, the lobe structure is significantly altered; in the longitudinal plane there is relatively small change, but in the transverse plane the central lobe is broadened to approximately $2\psi_m$. For angles of incidence past $\pm\psi_m$ in the transverse plane, there is a sharp decrease in the envelope of the lobe structure.

II. General Formulation

For conducting surfaces, the scattered magnetic field in the wave zone is[6]

$$\vec{H}_{sc}(\vec{r}) = \frac{ike^{ikr}}{4\pi r} \left(\frac{\vec{r}}{r}\right) \times \left[\int_S dS' \left(\vec{n}(\vec{r}') \times \vec{H}(\vec{r}') \right) e^{-ik\left(\frac{\vec{r}}{r}\right) \cdot \vec{r}'} \right] \quad (1)$$

where the integration is over the complete scattering surface, $\vec{r}$ denotes the field point, $\vec{r}'$ denotes the surface point of integration, and $k = 2\pi/\lambda$ is the wave number. (The origin of coordinates is assumed to be near the scatterer.)

Generally the correct field on the surface is not known and the integral cannot be evaluated. However, experience with the problem of reflection by an infinite plane suggests the Kirchhoff approximation which, in fact, yields reasonable results for surfaces characteristically very large compared to a wavelength. For an incident plane wave this approximation is

$$\vec{n}(\vec{r}') \times \vec{H}(\vec{r}') \simeq \begin{cases} 2\vec{n}(\vec{r}') \times \vec{H}_{inc}(\vec{r}') & \text{on the illuminated portion} \\ 0 & \text{on the geometric shadow} \end{cases}$$

where

$$\vec{H}_{inc}(\vec{r}') = \vec{\epsilon}\, H_o e^{i\vec{k} \cdot \vec{r}'} ,$$

$\vec{\epsilon}$ is the transmitted polarization, H_o is a constant, $\vec{k}$ is a vector of magnitude k in the incident direction and $\vec{k} \cdot \vec{\epsilon} = 0$.

For the radar problem, the backscattered field is to be evaluated; thus,

$$\left(\frac{\vec{r}}{r}\right) = -\left(\frac{\vec{k}}{k}\right) .$$

Using the fact that

$$\vec{k} \times (\vec{n} \times \vec{\epsilon}) = \vec{n}(\vec{k} \cdot \vec{\epsilon}) - \vec{\epsilon}(\vec{k} \cdot \vec{n}) = - \vec{\epsilon}(\vec{k} \cdot \vec{n}) \quad ,$$

the resulting expression for the backscattered field is

$$\vec{H}_{bsc}(r) = \vec{\epsilon} \frac{iH_o e^{ikr}}{2\pi r} \int_S dS' \, \vec{k} \cdot \vec{n}(\vec{r}') \, e^{i2\bar{k} \cdot \bar{r}'} \quad , \tag{2}$$

where the integration is now to be performed only over the illuminated surface. (It is to be noted that in this approximation the polarization of the back-scattered field is identical to that of the incident field.)

Finally, the radar cross section is calculated by

$$\sigma = 4\pi r^2 \frac{|\vec{H}_{bsc}(r)|^2}{|\vec{H}_{inc}(r)|^2} \tag{3}$$

III. Flat Plates

The cross section (normalized to λ^2) for reflection from large flat plates[1] is given here in order to compare with the results for curved plates (Fig. 1 indicates the geometry where φ is the azimuth of $\vec{k}$ in the y = 0 plane).

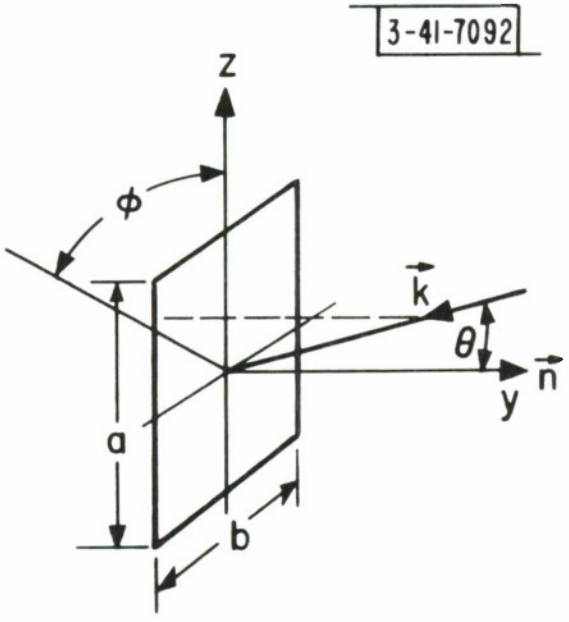

Fig. 1

$$\frac{\sigma(\theta,\varphi)}{\lambda^2} = 4\pi\left(\frac{a}{\lambda}\right)^2\left(\frac{b}{\lambda}\right)^2 \cos^2\theta\left(\frac{\sin(ka\cos\varphi\sin\theta)}{ka\cos\varphi\sin\theta}\right)^2\left(\frac{\sin(kb\sin\varphi\sin\theta)}{kb\sin\varphi\sin\theta}\right)^2 . \quad (4)$$

Characteristic of large flat plates, this pattern contains a large central peak ($\theta \sim 0$) and sidelobes rapidly decreasing as θ increases from zero. For $\varphi = 0$ or $\pi/2$, the sidelobes decrease as $\sin^2 x/x^2$ for $x = ka \sin\theta$ or $kb \sin\theta$, respectively.

IV. Curved Plates

Figures 2a and 2b indicate the geometry and coordinate system to be used in the calculations for curved plates. As shown in the diagram the incident wave approaches the concave side of the plate. Although the scattered field in the vicinity of the plate (radial distances of the order of radius of curvature of the plate) may show focusing tendencies, there is no focusing in the wave zone. It is shown in Appendix A that the radar cross section for scattering from the convex side is equal to that for scattering from the concave side.

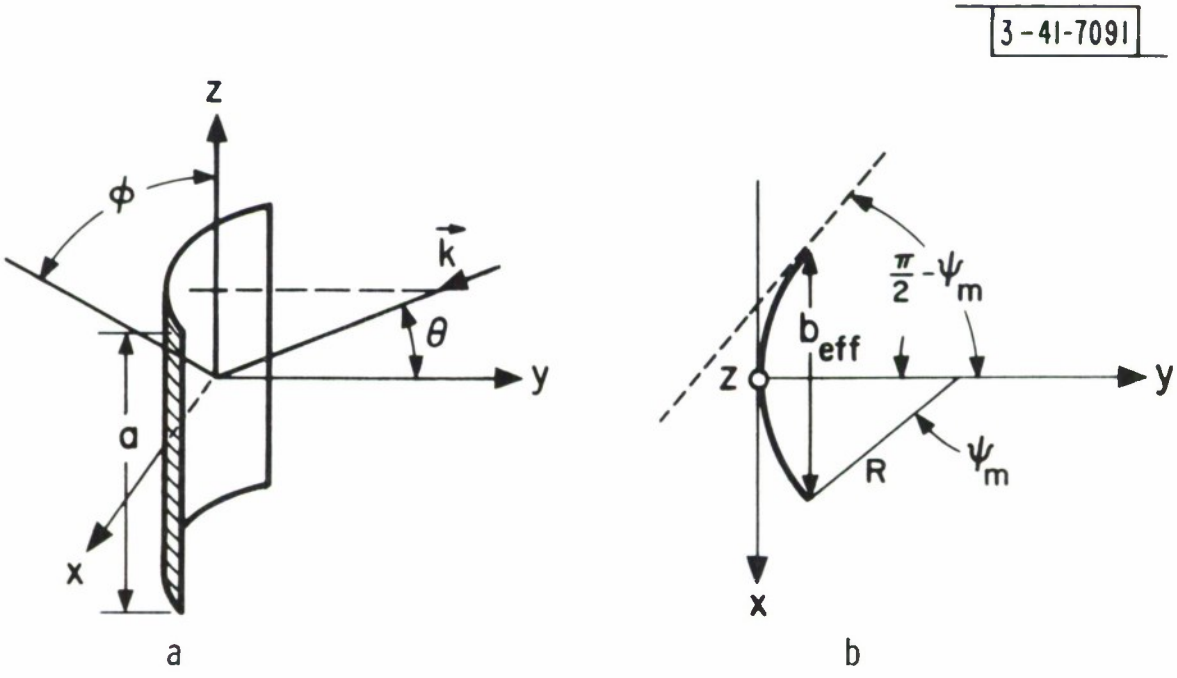

Fig. 2

The effective width, or aperture width, is

$$b_{eff} = 2R \sin \psi_m \ ;$$

the aperture depth is

$$d = R(1 - \cos \psi_m) \ ;$$

and the limiting case for a flat plate is simply $R \to \infty$, $\psi_m \to 0$, such that b_{eff}

remains constant and equal to b, the width of the equivalent flat plate, while $d \to 0$.

To treat the concave side, the geometry shown in Figs. 2a and 2b implies that

$$\vec{r}' = \vec{x}R \sin \psi + \vec{y}R(1 - \cos \psi) + \vec{z}z,$$

$$\vec{n}(\vec{r}') = -\vec{x} \sin \psi + \vec{y} \cos \psi,$$

$$\vec{k}/k = -\vec{x} \sin \varphi \sin \theta - \vec{y} \cos \theta - \vec{z} \cos \varphi \sin \theta,$$

where $\vec{x}$, $\vec{y}$, $\vec{z}$ are the unit coordinate vectors. Equation (2) may then be reduced to the form

$$\vec{H}_{bsc}(r) = \vec{\epsilon} \frac{-ikH_o e^{i(kr - 2kR \cos \theta)}}{2\pi r} \left(\int_{-a/2}^{a/2} dz\, e^{-i2kz \cos \varphi \sin \theta} \right) \times$$

$$\left(\int_{-\psi_m}^{\psi_m} Rd\psi(\cos \theta \cos \psi - \sin \theta \sin \varphi \sin \psi) e^{i2kR(\cos \theta \cos \psi - \sin \theta \sin \varphi \sin \psi)} \right).$$

(It has been assumed that

$$-\left(\frac{\pi}{2} - \psi_m\right) \leq \theta \leq +\left(\frac{\pi}{2} - \psi_m\right)$$

so that the convex side of the plate is always in the geometric shadow.) The z integration may be performed leaving

$$\vec{H}_{bsc}(r) = \vec{\epsilon} \frac{-ika\, H_o e^{i(kr - 2kR \cos \theta)}}{2\pi r} \left| \frac{\sin (ka \cos \varphi \sin \theta)}{ka \cos \varphi \sin \theta} \right| \times$$

$$\int_{-\psi_m}^{\psi_m} Rd\psi(\cos \theta \cos \psi - \sin \theta \sin \varphi \sin \psi) e^{i2kR(\cos \theta \cos \psi - \sin \theta \sin \varphi \sin \psi)} . \qquad (5)$$

Let

$\rho = 2kR;$

then

$$\vec{H}_{bsc}(r) = \vec{\epsilon}\,\frac{-ka\,R\,H_o e^{i(kr - \rho\cos\theta)}}{2\pi r}\left(\frac{\sin(ka\cos\varphi\sin\theta)}{ka\cos\varphi\sin\theta}\right)\frac{\partial}{\partial\rho}I(\rho,\psi_m,\theta,\varphi), \tag{6}$$

where

$$I(\rho,\psi_m,\theta,\varphi) = \int_{-\psi_m}^{\psi_m} d\psi\, e^{i\rho(\cos\theta\cos\psi - \sin\theta\sin\varphi\sin\psi)}\,. \tag{7}$$

The function $I(\rho,\psi_m,\theta,\varphi)$ contains most of the effect of curvature. In the limiting case of a flat plate, it is shown in Appendix B that

$$R\frac{\partial}{\partial\rho}I(\rho,\psi_m,\theta,\varphi) \xrightarrow[\substack{R\to\infty\\ \psi_m\to 0\\ b = 2R\psi_m}]{} ib\cos\theta\left(\frac{\sin(kb\sin\varphi\sin\theta)}{kb\sin\varphi\sin\theta}\right)e^{i2kR\cos\theta}\,. \tag{B-2}$$

Using this result in Eq. (6) and calculating the radar cross section by Eq. (3) yields the quoted result in Eq. (4). For the present case of interest, b_{eff}/λ is to be considered large; however, ψ_m is too large to consider the trigonometric expansions used for the flat plate limit. The resulting expression would appear as a series in products of powers of ρ and of ψ_m. Thus it is necessary to develop a new evaluation for $R \to \infty$ while ψ_m remains finite.

If $\varphi = 0$, the function $I(\rho,\psi_m,\theta,0)$ is closely related to the integral representation for the Bessel function of zeroth order, i.e., for $\psi_m = \pi$ corresponding to the closed cylinder, we find

$$I(\rho,\psi_m = \pi,\theta,\varphi = 0) = \frac{1}{2\pi}J_o(\rho\cos\theta)\,.$$

In spite of this suggestive relation, it does not seem possible to find such a simple result for ψ_m in the more interesting range of 10° to 30°. Furthermore, for φ not too near 0 or $\pi/2$ the sin ψ term in the exponent greatly complicates

the problem. It is possible to treat the cases $\varphi = 0$ and $\varphi = \pi/2$ by appropriately expanding the integrand,* but it is not possible to justify the results consistently (i.e., to show that succeeding terms may be neglected). Treating only these two cases, we shall employ techniques of deforming the ψ contour into an appropriate complex plane. In this way a consistent expansion for $R \to \infty$ and ψ_m finite may be determined.

---

*One may proceed by expanding $e^{i\rho \cos\theta \cos\psi}$ in a Fourier series with Bessel function coefficients. Using the asymptotic form (for $t = \rho \cos\theta \to \infty$) of $J_n(t)$, one may then re-sum the series to find

$$\frac{\partial}{\partial\rho} I(\rho,\psi_m,\theta,\varphi = 0) \xrightarrow[\rho \to \infty]{} \cos\theta \sqrt{\frac{2\pi}{\rho}}\, e^{i(\rho \cos\theta + \pi/4)} \quad \text{for } 0 < \psi_m < \pi/2.$$

However, following the same procedure with the next term in the asymptotic expansion of $J_n(t)$ of order $\rho^{-3/2}$, leads to an indeterminate result.

The same procedure, when applied for the case $\varphi = \pi/2$, leads to the result

$$\frac{\partial}{\partial\rho} I(\rho,\psi_m,\theta,\tfrac{\pi}{2}) \xrightarrow[\rho \to \infty]{} \sqrt{\frac{2\pi}{\rho}}\, e^{i(\rho + \pi/4)} \begin{cases} 0 & -(\pi/2 - \psi_m) \le \theta < -\psi_m \\ 1 & -\psi_m \le \theta \le \psi_m \\ 0 & \psi_m < \theta \le (\pi/2 - \psi_m) \end{cases}$$

This result is very interesting since it corresponds to geometrical optics which implies a constant cross section confined to the region for which the incident wave is normal to part of the plate. Investigation of the $\rho^{-3/2}$ term again leads to an indeterminate result.

A. Longitudinal Case ($\varphi = 0$)

For $\varphi = 0$, the projection of $\vec{k}$ in the $y = 0$ plane is parallel to the elements of the cylinder. Equation (6) indicates that a dominant part of the lobing structure will arise from the flat-plate term $\frac{1}{x} \sin x$, where $x = ka \sin \theta$. The problem is thus reduced to evaluating ($\varphi = 0$ denoted by superscript)

$$I''(\rho, \psi_m, \theta) = \int_{-\psi_m}^{\psi_m} d\psi \, e^{i\rho \cos \theta \cos \psi} . \tag{8}$$

If one defines

$$z = \cos \psi \text{ and } t = \rho \cos \theta,$$

the integral may easily be transformed into

$$I''(\rho, \psi_m, \theta) = 2 \int_{\cos \psi_m}^{\prime} \frac{dz e^{itz}}{\sqrt{1 - z^2}} . \tag{9}$$

With cuts in the complex z-plane on the complete imaginary axis and on the real axis from $z = 1$ to $z = \infty$,

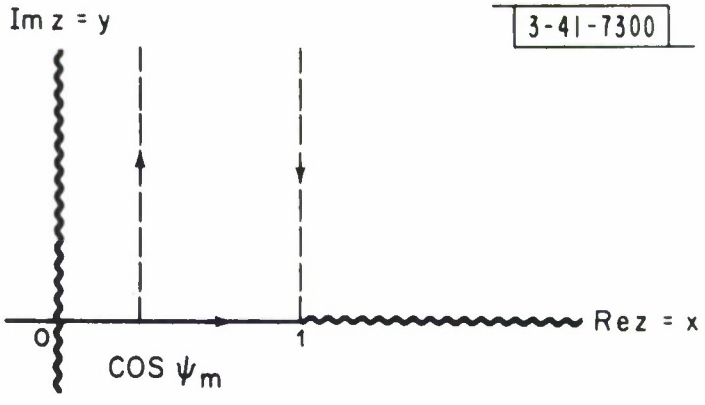

Fig. 3

the contour may be conveniently deformed into that shown by dashed lines in Fig. 3, up the line $x = \cos \psi_m$ and down the line $x = 1$. The joining line at $y = \infty$ gives no contribution due to the convergent factor $e^{-ty} \underset{y \to \infty}{\to} 0$. Along these two lines the exponent is real and provides maximum convergence.[7] The resulting expression for the integral is

$$I''(t,\psi_m) = 2ie^{it \cos \psi_m} \int_0^\infty dy \frac{e^{-ty}}{\sqrt{1 - (\cos \psi_m + iy)^2}} - 2ie^{it} \int_0^\infty dy \frac{e^{-ty}}{\sqrt{1 - (1 + iy)^2}} \qquad (10)$$

First consider the term due to integration along $x = \cos \psi_m$ and expand the denominator about $y = 0$. One finds

$$\int_0^\infty dy \frac{e^{-ty}}{\sqrt{1 - (\cos \psi_m + iy)^2}}$$

$$= \int_0^\infty dy\, e^{-ty} \frac{1}{\sin \psi_m} \left[1 + y \frac{i \cos \psi_m}{\sin^2 \psi_m} - \frac{y^2}{2 \sin^2 \psi_m} \left(1 + \frac{3 \cos^2 \psi_m}{\sin^2 \psi_m} \right) + \ldots \right]$$

$$= \frac{1}{t \sin \psi_m} \left[1 + \frac{i \cos \psi_m}{t \sin^2 \psi_m} - \frac{(\sin^2 \psi_m + 3 \cos^2 \psi_m)}{t^2 \sin^4 \psi_m} + \ldots \right] .$$

This series is apparently convergent as $t \to \infty$ and ψ_m remains constant and is a useful result for $t \sin^2 \psi_m = 2kR \cos \theta \sin^2 \psi_m \gg 1$. To evaluate the

contributions from integration along x = 1, factor the denominator into two terms

$$\frac{1}{\sqrt{1 - (1 + iy)^2}} = \frac{1}{\sqrt{y^2 - 2iy}} = \frac{1}{\sqrt{y}\ \sqrt{y - 2i}} \quad .$$

Expanding the factor $1/\sqrt{y - 2i}$ about $y = 0^+$ (i. e., $y \to 0$ from above the cut at $y = 0$, $x = 1$) the result of integration is

$$\int_0^\infty dy\ \frac{e^{-ty}}{\sqrt{1 - (1 + iy)^2}} = \frac{e^{i\,\pi/4}}{\sqrt{2}} \int_0^\infty dy\ \frac{e^{-ty}}{\sqrt{y}} \left(1 - \frac{iy}{4} - \frac{y^2}{8} + \ldots\right)$$

$$= e^{i\,\pi/4} \sqrt{\frac{\pi}{2t}} \left(1 - \frac{i}{8t} \left(1 - \frac{i}{8t} - \frac{3}{32t^2} + \ldots\right)\right) \quad .$$

This series is also apparently convergent as $t \to \infty$. In fact, even if it is an asymptotic series one may assume that $1/\sqrt{y - 2i}$ has a convergent expansion for $|y| < 2$. Then contributions for $y \geq 2$ for large t may be bounded as follows:

$$\left| \int_2^\infty \frac{e^{-ty}}{\sqrt{y^2 - 2iy}} \right| = \int_2^\infty \frac{dy\ e^{-ty}}{(y^4 + 4y^2)^{1/4}} \leq \int_2^\infty dy\ e^{-ty} = \frac{e^{-2t}}{t} \underset{t \to \infty}{\to} 0 \quad .$$

Finally,

$$I''(t, \psi_m) = 2ie^{it \cos \psi_m} \frac{1}{t \sin \psi_m} \left(1 + \frac{i \cos \psi_m}{t \sin^2 \psi_m} + \ldots\right)$$

$$- 2ie^{i(t + \pi/4)} \sqrt{\frac{\pi}{2t}} \left(1 - \frac{i}{8t} + \ldots\right) , \qquad (11)$$

and keeping only the two lowest order terms

$$\frac{\partial}{\partial\rho} I''(\rho,\psi_m,\theta) \xrightarrow[\rho \to \infty]{} \cos\theta \frac{2\pi}{\sqrt{\rho \cos\theta}} e^{i(\rho \cos\theta + \pi/4)}$$

$$- \frac{2\cos\theta}{\rho \cos\theta \tan\psi_m} e^{i\rho \cos\theta \cos\psi_m} . \qquad (12)$$

Using Eq. (12) in Eq. (6),

$$H''_{bsc}(r) \xrightarrow[R \to \infty]{} \frac{-ka\, R\, H_o e^{i(kr - 2kR\cos\theta)}}{2\pi r} \cos\theta \left(\frac{\sin(ka\sin\theta)}{ka\sin\theta}\right) \cdot$$

$$\left[\sqrt{\frac{\pi}{kR\cos\theta}} e^{i(2kR\cos\theta + \pi/4)} - \frac{1}{kR\cos\theta\tan\psi_m} e^{i2kR\cos\theta\cos\psi_m}\right] . \qquad (13)$$

Finally, Eq. (3) yields

$$\frac{\sigma''(\theta)}{\lambda^2} = \frac{4\pi r^2}{\lambda^2} \frac{|H_{bsc}(r)|^2}{|H_{inc}(r)|^2}$$

$$\xrightarrow[R \to \infty]{} 2\pi\left(\frac{a}{\lambda}\right)^2\left(\frac{R}{\lambda}\right)\cos\theta \left[\frac{\sin(ka\sin\theta)}{ka\sin\theta}\right]^2 \left[1 - \frac{2\cos\left(4kR\sin^2\frac{\psi_m}{2}\cos\theta + \frac{\pi}{4}\right)}{\pi\sqrt{2\left(\frac{R}{\lambda}\right)\cos\theta\tan\psi_m}}\right] \qquad (14)$$

which is valid for $2kR \cos\theta \sin^2 \psi_m >> 1$. One may now compare this result with that for a flat plate for $\varphi = 0$ given in Eq. (4) to find that the basic lobe structure is identical. Furthermore, neglecting the second term in Eq. (14) indicates that the peak is reduced by

$$\frac{\sigma''(\theta = 0)}{\sigma_{fl.pl.}(\theta = 0)} \underset{R \to \infty}{\sim} \frac{2\pi(\frac{a}{\lambda})^2(\frac{R}{\lambda})}{4\pi(\frac{a}{\lambda})^2(\frac{b_{eff}}{\lambda})^2} = \frac{1}{8(\frac{R}{\lambda}) \sin^2 \psi_m} .$$

The second term, for θ not too near $\pi/2$, serves to add a small, slow oscillation about the dominant lobe structure. The effect of the curvature seems to reduce the coherent scattering area to a strip near the central element of the cylinder and thus to reduce the peak radar cross section.

Figures 5 through 8 show four examples for calculations of $\sigma''(\theta)$ given by Eq. (14). Since the correction terms for these examples have a period much longer than the flat-plate lobe structure, one may only detect a reduction of the central peaks.

B. Transverse Case ($\varphi = \pi/2$)

For $\varphi = \pi/2$, the projection of $\hat{k}$ in the $y = 0$ plane is perpendicular to all similarly projected elements of the cylinder. Equation (6) indicates that the flat-plate lobe structure is absent and thus implies the importance of the structure integral to be evaluated. For $\varphi = \pi/2$ (labeled by $\perp$ superscript),

$$I^{\perp}(\rho, \psi_m, \theta) = \int_{-\psi_m}^{\psi_m} d\psi \, e^{i\rho \cos(\psi + \theta)} \quad . \tag{15}$$

The θ dependence of $I^{\perp}$ is much more complicated than that of I''. If one proceeds in a way similar to that for I'', one is immediately faced with the fact that the integrand on the lines $x = \cos \psi_m$ and $x = 1$ still has a rapidly oscillating factor. Furthermore, it seems too difficult to find and use the appropriate stationary phase contours passing through the points $x = \cos \psi_m$, $y = 0$ and $x = 1$, $y = 0$.

It is possible to rearrange $I^{\perp}(\rho, \psi_m, \theta)$ as two separate integrals as follows:

$$I^{\perp}(\rho, \psi_m, \theta) = \int_{-\psi_m}^{\psi_m} d\psi \, e^{i\rho \cos(\psi + \theta)}$$

$$= \int_{-\psi_m + \theta}^{\psi_m + \theta} d\psi \, e^{i\rho \cos \psi}$$

$$= \int_{0}^{\psi_m + \theta} d\psi \, e^{i\rho \cos \psi} + \int_{0}^{\psi_m - \theta} d\psi \, e^{i\rho \cos \psi} \quad .$$

Now the two regions $|\theta| < \psi_m$, $|\theta| > \psi_m$, and the points $|\theta| = \psi_m$ may be considered separately, and the results of the previous evaluation for $I^{//}(\rho,\psi_m,\theta)$ are sufficient to determine $I^{\perp}(\rho,\psi_m,\theta)$. The results for $|\theta| < \psi_m$ will diverge (negative infinite) as $|\theta| \to \psi_m$; the results for $|\theta| > \psi_m$ will diverge (positive infinite) as $|\theta| \to \psi_m$; but, the result for $|\theta| = \psi_m$ will provide a reasonable joining point between the two regions. Furthermore, the results for $|\theta| > \psi_m$ must also be limited to $|\theta| \leq \frac{\pi}{2} - \psi_m$; Fig. 2b indicates that for $|\theta| > \frac{\pi}{2} - \psi_m$ part of the concave side is then geometrically shadowed and part of the convex side is illuminated by the incident wave.

1) $\underline{|\theta| < \psi_m}$

For $|\theta| < \psi_m$, let $z = \cos\psi$ to yield

$$I^{\perp}(\rho,\psi_m,\theta) = ie^{i\rho\cos(\psi_m+\theta)} \int_0^\infty dy \frac{e^{-ty}}{\sqrt{1 - \left[\cos(\psi_m + \theta) + iy\right]^2}}$$

$$+ ie^{i\rho\cos(\psi_m-\theta)} \int_0^\infty dy \frac{e^{-ty}}{\sqrt{1 - \left[\cos(\psi_m - \theta) + iy\right]^2}}$$

$$- 2ie^{i\rho} \int_0^\infty dy \frac{e^{-\rho y}}{\sqrt{1 - (1 + iy)^2}} \qquad (17)$$

Comparison with Eqs. 9, 10, 12 and 14 leads immediately to the results

$$\frac{\partial}{\partial\rho} I(\rho,\psi_m,\theta) \xrightarrow[\rho \to \infty]{}$$

$$\sqrt{\frac{2\pi}{\rho}}\; e^{i(\rho+\pi/4)} - \left\{ \frac{e^{i\rho\,\cos(\psi_m + \theta)}}{\rho\,\tan(\psi_m + \theta)} + \frac{e^{i\rho\cos(\psi_m - \theta)}}{\rho\,\tan(\psi_m - \theta)} \right\}$$

and

$$\frac{\sigma^{\perp}(\theta)}{\lambda^2} \xrightarrow[R \to \infty]{} 2\pi\left(\frac{a}{\lambda}\right)^2 \left(\frac{R}{\lambda}\right) \left[1 - \frac{1}{\pi\sqrt{2\frac{R}{\lambda}}} \left\{ \frac{\cos\left[4kR\,\sin^2\left(\frac{\psi_m+\theta}{2}\right) + \frac{\pi}{4}\right]}{\tan\,(\psi_m + \theta)} \right.\right.$$

$$\left.\left. + \frac{\cos\left[4kR\,\sin^2\,\left(\frac{\psi_m-\theta}{2}\right) + \frac{\pi}{4}\right]}{\tan\,(\psi_m - \theta)} \right\} \right] . \qquad (18)$$

2) $\underline{|\theta| = \psi_m}$

For $|\theta| = \psi_m$, one of the contours is absent and the other runs from $0 \le \psi \le 2\psi_m$ (or $0 \ge \psi \ge -2\psi_m$). Letting $z = \cos\psi$,

$$I^{\perp}(\rho, \psi_m, \theta) = ie^{i\rho\,\cos\,2\psi_m} \int_0^{\infty} dy\, \frac{e^{-ty}}{\sqrt{1 - \left[\cos\,2\psi_m + iy\right]^2}}$$

$$- ie^{i\rho} \int_0^{\infty} dy\, \frac{e^{-ty}}{\sqrt{1 - (1 + iy)^2}} \quad . \qquad (19)$$

Again comparing with Eqs. (9), (10), (12) and (14) leads to

$$\frac{\partial}{\partial\rho}\; I^{\perp}(\rho, \psi_m, \theta = \psi_m) \xrightarrow[\rho \to \infty]{} \sqrt{\frac{\pi}{2\rho}}\; e^{i(\rho+\pi/4)} - \frac{e^{i\rho\,\cos\,2\psi_m}}{\rho\,\tan\,2\psi_m}$$

and

$$\frac{\sigma^{\perp}(\theta = \psi_m)}{\lambda^2} \xrightarrow[R \to \infty]{} 2\pi\left(\frac{a}{\lambda}\right)^2 \left(\frac{R}{\lambda}\right) \left[\frac{1}{4} - \frac{\cos(4kR \sin^2 \psi_m + \frac{\pi}{4})}{2\pi\sqrt{2\frac{R}{\lambda}} \tan 2\psi_m}\right] . \quad (20)$$

3) $\frac{\pi}{2} - \psi_m \geq |\theta| > \psi_m$

Finally, for $|\theta| > \psi_m$ the two integrals in Eq. (16) should be recombined to yield (for $z = \cos \psi$)

$$I^{\perp}(\rho, \psi_m, \theta) = \int_{\theta-\psi_m}^{\theta+\psi_m} d\psi \, e^{i\rho \cos \psi}$$

$$= ie^{i\rho \cos(\theta + \psi_m)} \int_0^{\infty} dy \frac{e^{-ty}}{\sqrt{1 - [\cos(\theta + \psi_m) + iy]^2}}$$

$$- ie^{i\rho \cos(\theta-\psi_m)} \int_0^{\infty} dy \frac{e^{-ty}}{\sqrt{1 - [\cos(\theta-\psi_m) + iy]^2}} . \quad (21)$$

The same comparisons used above then yield

$$\frac{\partial}{\partial\rho} I^{\perp}(\rho, \psi_m, \theta) \xrightarrow[\rho \to \infty]{} \left[\frac{e^{i\rho \cos(\theta-\psi_m)}}{\rho \tan(\theta-\psi_m)} - \frac{e^{i\rho \cos(\theta+\psi_m)}}{\rho \tan(\theta+\psi_m)}\right],$$

and

$$\frac{\sigma^{\perp}(\theta)}{\lambda^2} \xrightarrow[R \to \infty]{} \frac{1}{4\pi}\left(\frac{a}{\lambda}\right)^2 \left[\frac{1}{\tan^2(\theta-\psi_m)} + \frac{1}{\tan^2(\theta+\psi_m)}\right.$$

$$\left. - \frac{2 \cos(4kR \sin \psi_m \sin \theta)}{\tan(\theta-\psi_m) \tan(\theta+\psi_m)}\right] . \quad (22)$$

As previously mentioned, $\sigma'(\theta)$ does not contain the flat-plate lobe structure. In fact, for $R/\lambda >> 1$, Eqs. (18) and (20) indicate $\sigma'(\theta)$ is roughly constant falling to about 1/4 the central value at $|\theta| = \psi_m$. Equation (22) then implies a further rapid decrease as $|\theta| \to \frac{\pi}{2} - \psi_m$; near this limit the oscillatory term should be apparent due to the occurrence of only one power of the diverging tangent function in the denominator. Figures 9 through 12 bear out these observations for several combinations of ψ_m and (R/λ). Also included in each figure is the result one obtains for the equivalent flat plate result (using $b = b_{eff} = 2R \sin \psi_m$ in Eqs. (B-2) and (4)).

V. Conclusions

One may observe from Figs. 5 through 12 that calculations which appropriately account for the curvature of the plate show that the central lobe region is effectively reduced in magnitude by the factor $1/8(R/\lambda) \sin^2 \psi_m$; the angular width of this region is broadened to approximately $2\psi_m$ in the transverse plane. Thus, in the case of radar backscattering, a small curvature in the plate (large R) may lead to an appreciable reduction in the peak cross section by distributing the energy more evenly. Although only single curvature has been considered, it seems reasonable to suspect that a doubly curved surface (both curvatures being small) will further reduce the peak cross section; however, calculations are necessary to support this speculation.

APPENDIX A: Relation of the Field Scattered From the Convex Side to That Scattered From the Concave Side.

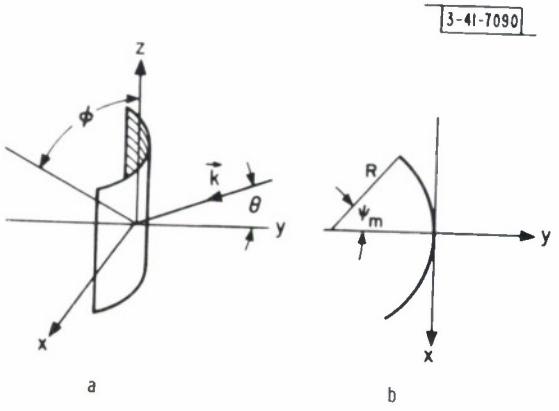

Fig. 4

The geometry shown in Figs. 4a and 4b indicates

$$\vec{r}' = -\vec{x}R \sin\psi - \vec{y}\,R(1 - \cos\psi) + \vec{z}z$$

$$\vec{n}(r') = -\vec{x} \sin\psi + \vec{y} \cos\psi$$

$$\vec{k}/k = -\vec{x} \sin\varphi \sin\theta - \vec{y} \cos\theta - \vec{z} \cos\varphi \sin\theta.$$

Equation (2) then reduces to the form

$$\vec{H}^{(\text{convex})}_{\text{bsc}}(r) = \vec{\epsilon}\,\frac{-ikH_o e^{i(kr + 2kR\cos\theta)}}{2\pi r}\left(\int_{-a/2}^{a/2} dz\, e^{-i2kz\cos\varphi\sin\theta}\right)$$

$$\left(\int_{-\psi_m}^{\psi_m} R\, d\psi(\cos\theta\cos\psi - \sin\theta\sin\varphi\sin\psi)\, e^{-i2kR(\cos\theta\cos\psi - \sin\theta\sin\varphi\sin\psi)}\right)$$

and after performing the z-integration

$$H_{bsc}^{(convex)}(r) = \vec{\epsilon}\,\frac{-ika\,H_o e^{i(kr+2kR\cos\theta)}}{2\pi r}\left(\frac{\sin(ka\cos\varphi\sin\theta)}{ka\cos\varphi\sin\theta}\times\right.$$

$$\left.\int_{-\psi_m}^{\psi_m} Rd\psi(\cos\theta\cos\psi-\sin\theta\sin\varphi\sin\psi)\,e^{-i2kR(\cos\theta\cos\psi-\sin\theta\sin\varphi\sin\psi)}\right).$$

Comparison of this last expression with that of Eq. (5) now shows that except for a known phase, $\vec{H}_{bsc}^{(convex)}(r)$ is the complex conjugate of $\vec{H}_{bsc}^{(concave)}(r)$, i.e.,

$$\vec{H}_{bsc}^{(convex)}(r) = e^{i(2kr - \pi/2)}\,\vec{H}_{bsc}^{(concave)}(r)\,)^* \quad . \qquad \text{(A-1)}$$

With this relation, Eq. (3) finally yields

$$\sigma^{(convex)}(\theta\,,\,\varphi) = \sigma^{(concave)}(\theta,\,\varphi)\,. \qquad \text{(A-2)}$$

APPENDIX B: Flat Plate Limit

Consider the function $I(\rho,\psi_m,\theta,\varphi)$ in the limit $\rho = 2kR \to \infty$ and $\psi_m \to 0$, such that $2R\psi_m = b$, the width of the flat plate. Expanding the integrand for small ψ,

$$I(\rho,\psi_m,\theta,\varphi) = \int_{-\psi_m}^{\psi_m} d\psi\, e^{i\rho(\cos\theta\cos\psi - \sin\theta\sin\varphi\sin\psi)} \qquad (7)$$

$$= e^{i\rho\cos\theta} \int_{-\psi_m}^{\psi_m} d\psi\, e^{-i\rho\psi\sin\theta\sin\varphi} \left[e^{i\rho\cos\theta(-\frac{\psi^2}{2})+..)-\sin\theta\cos\varphi(-\frac{\psi^3}{3}..)} \right]$$

$$= e^{i\rho\cos\theta} \int_{-\psi_m}^{\psi_m} d\psi e^{-i\rho\psi\sin\theta\sin\varphi} \left[1+i\rho\frac{\psi^2}{2}\cos\theta+i\rho\frac{\psi^3}{3!}\sin\theta\cos\varphi + \ldots \right]$$

$$\longrightarrow 2\left(\frac{\sin(\rho\psi_m\sin\varphi\sin\theta)}{\rho\sin\varphi\sin\theta}\right) e^{i\rho\cos\theta} \quad . \qquad (B\text{-}1)$$

$\rho \to \infty$

$\psi_m \to 0$

$2R\psi_m = b$

Furthermore,

$$R\frac{\partial}{\partial\rho} I(\rho,\psi_m,\theta,\varphi) \longrightarrow i2R\cos\theta \left(\frac{\sin(\rho\psi_m\sin\varphi\sin\theta}{\rho\sin\varphi\sin\theta}\right) e^{i\rho\cos\theta}$$

$\rho \to \infty$

$\psi_m \to 0$

$2R\psi_m = b$

$$= ib\cos\theta \left(\frac{\sin(kb\sin\varphi\sin\theta}{kb\sin\varphi\sin\theta}\right) e^{i2kR\cos\theta} \quad . \qquad (B\text{-}2)$$

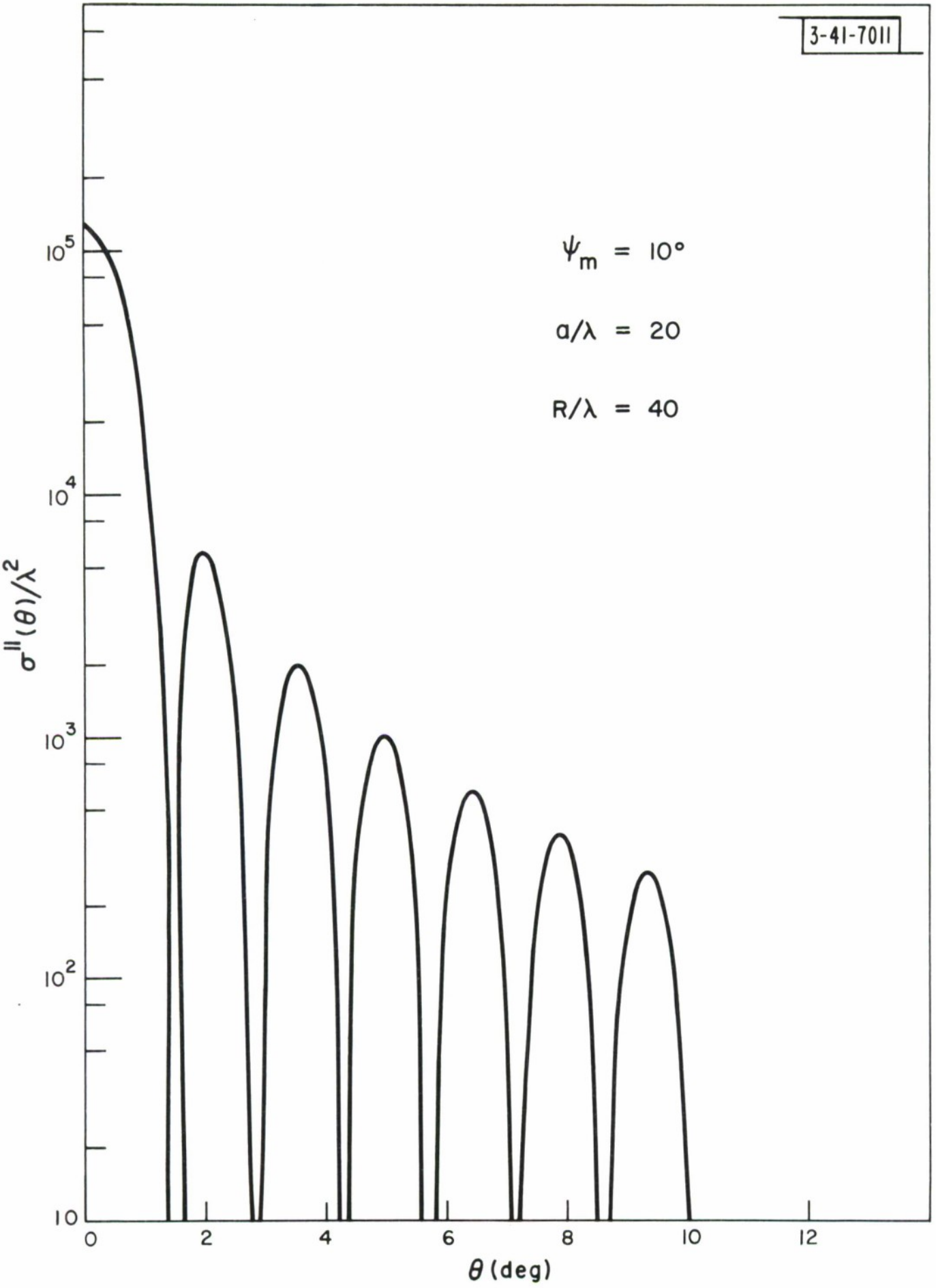
3-41-7011
$\psi_m = 10°$
$a/\lambda = 20$
$R/\lambda = 40$
10^5
10^4
10^3
10^2
10
$\sigma^{II}(\theta)/\lambda^2$
0
2
4
6
8
10
12
θ (deg)

Fig. 5

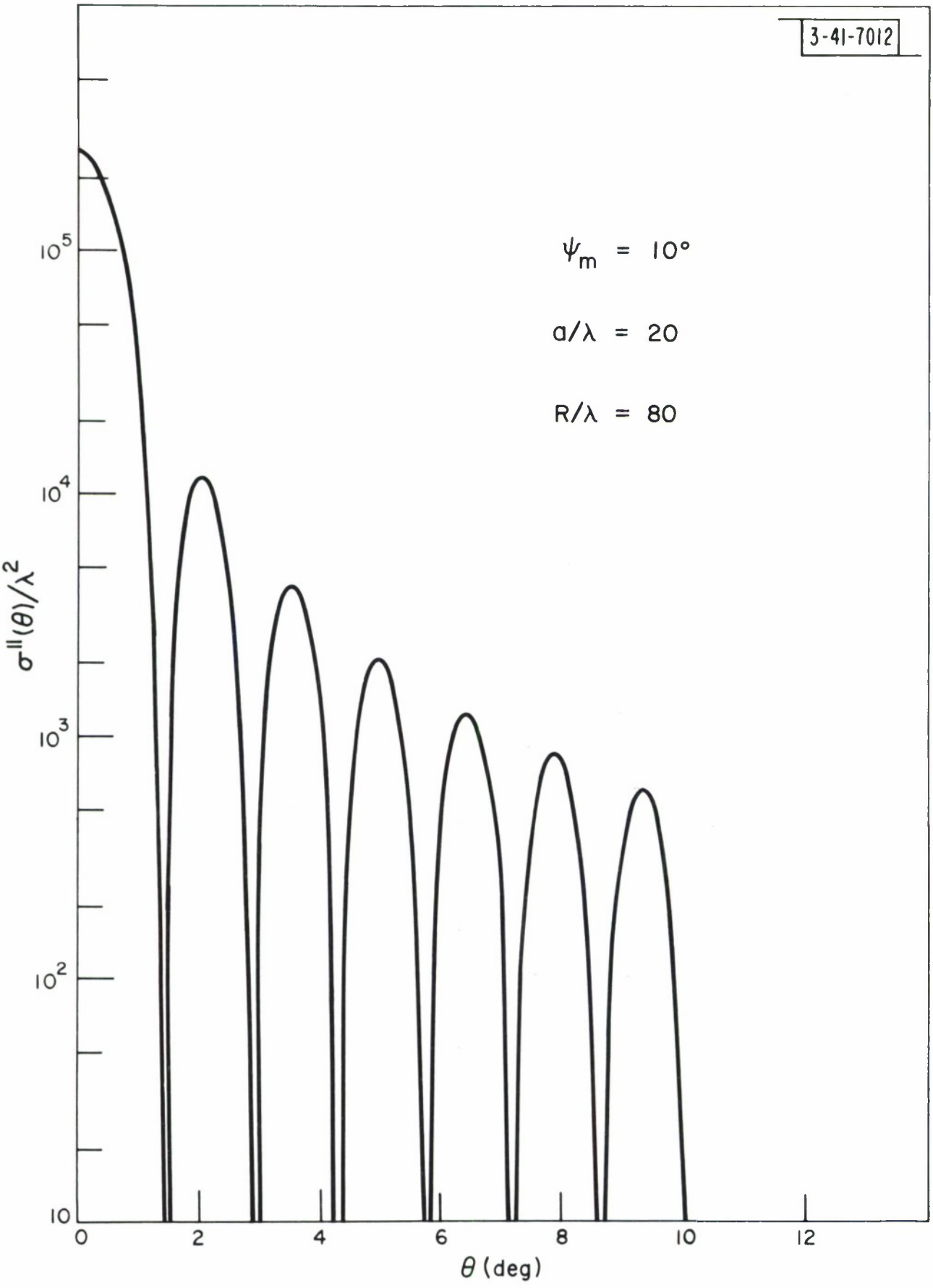
3-41-7012
ψ_m = 10°
a/λ = 20
R/λ = 80
10^5
10^4
10^3
10^2
10
$\sigma^{II}(\theta)/\lambda^2$
0
2
4
6
8
10
12
θ (deg)

Fig. 6

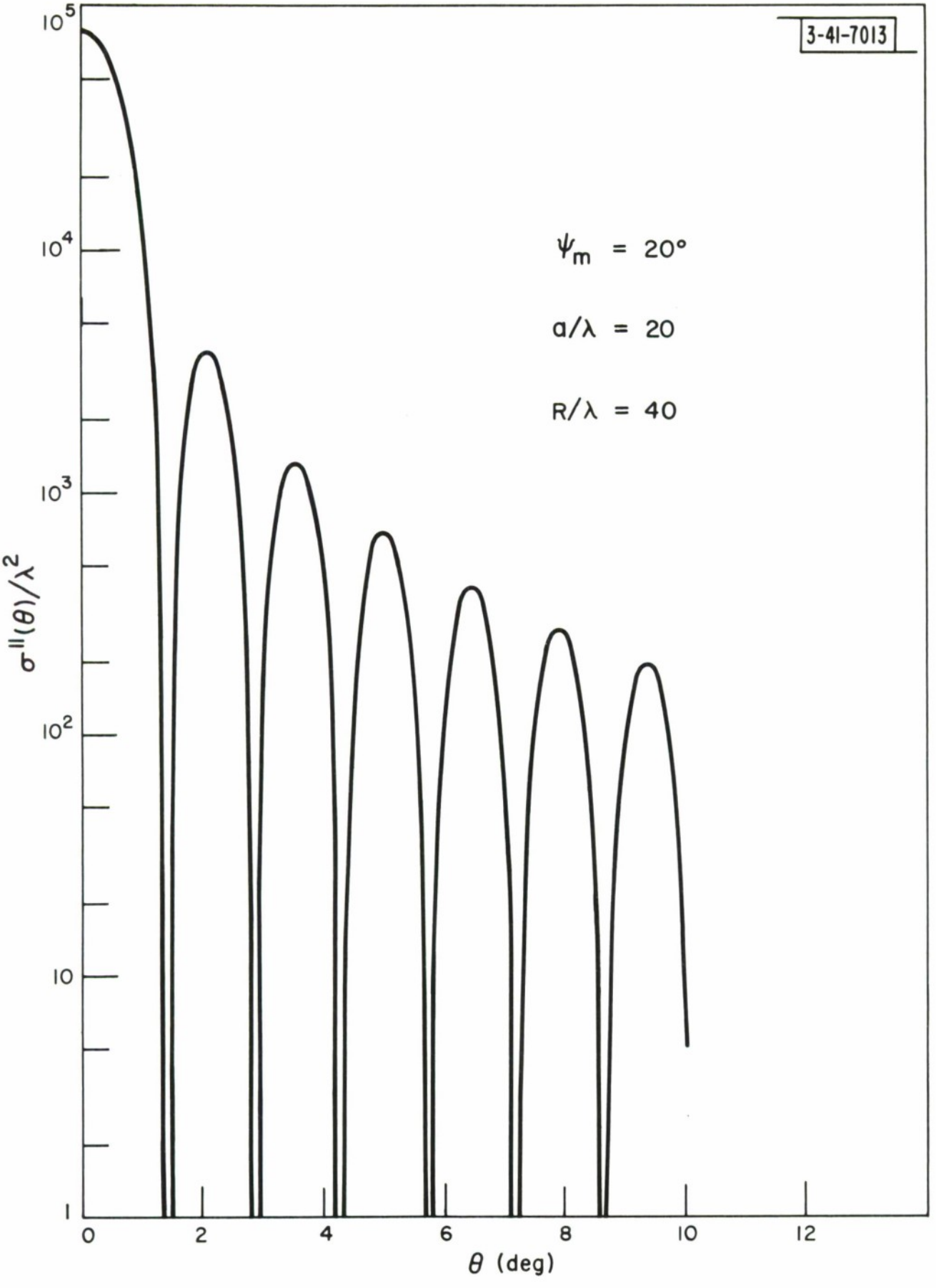
3-41-7013
$\psi_m = 20°$
$a/\lambda = 20$
$R/\lambda = 40$
$\sigma^{II}(\theta)/\lambda^2$
10^5
10^4
10^3
10^2
10
1
0
2
4
6
8
10
12
θ (deg)

Fig. 7

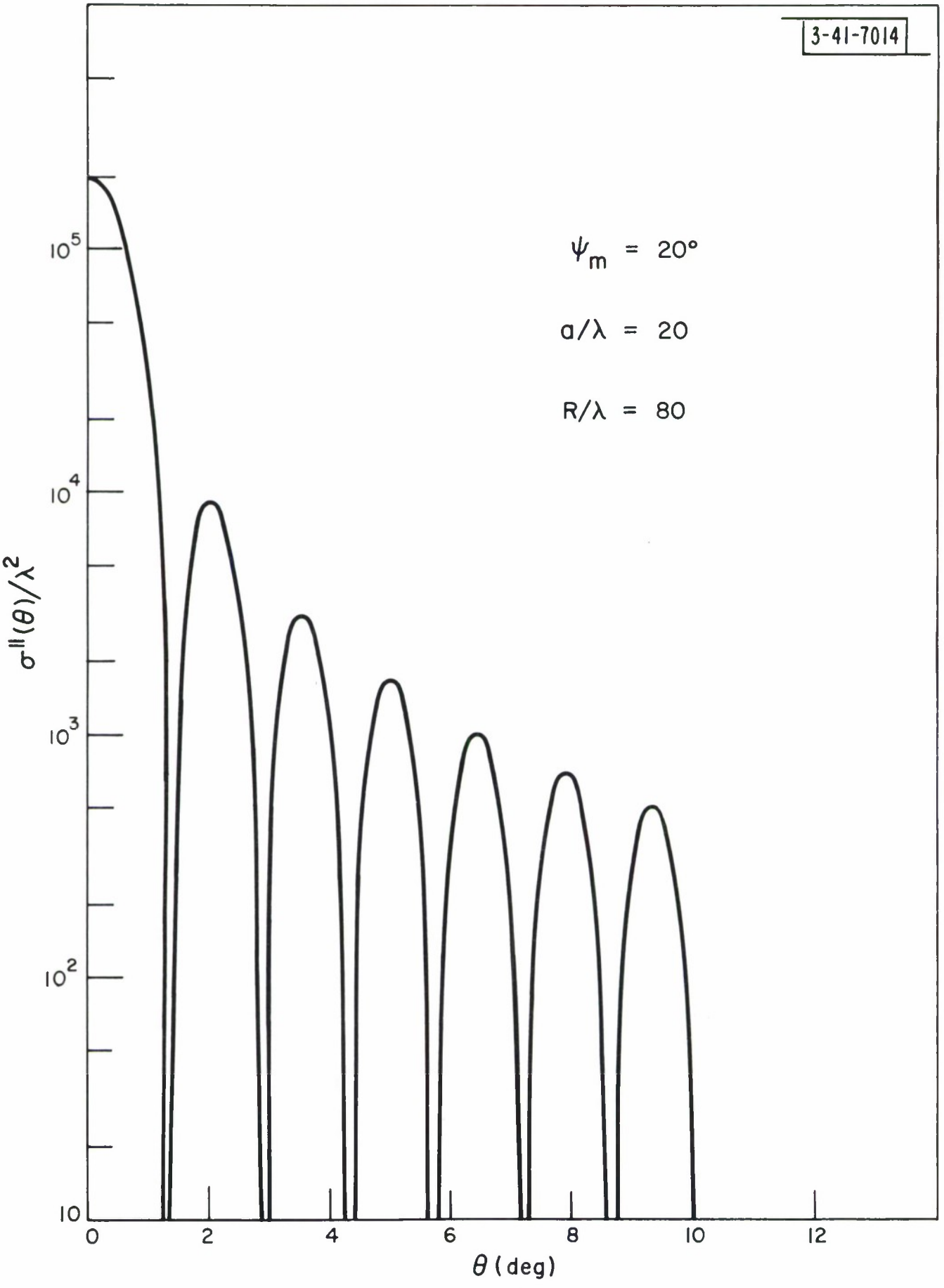
3-41-7014
ψ_m = 20°
a/λ = 20
R/λ = 80
10^5
10^4
10^3
10^2
10
$\sigma^{II}(\theta)/\lambda^2$
0
2
4
6
8
10
12
θ (deg)

Fig. 8

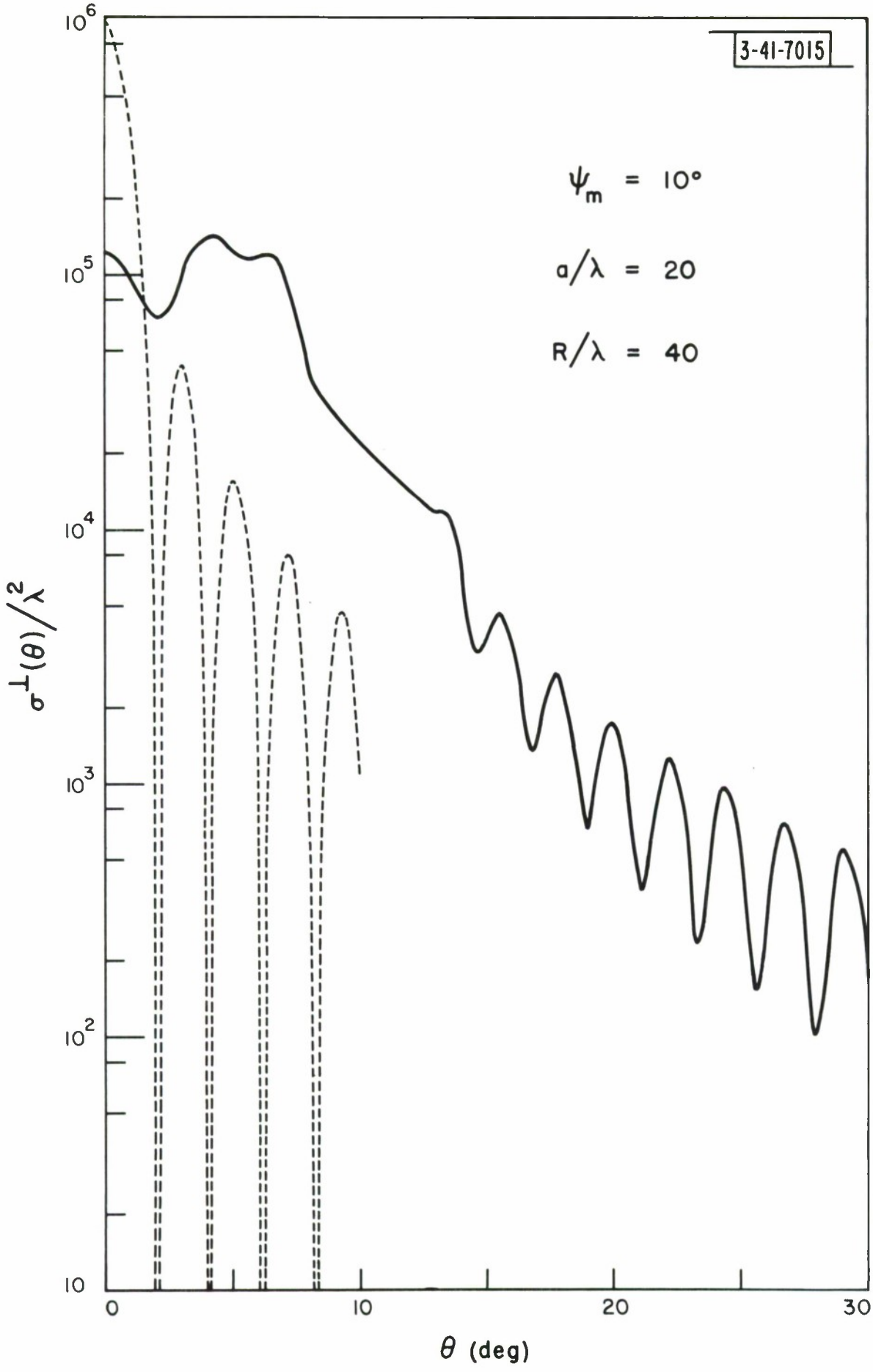
3-41-7015
ψ_m = 10°
a/λ = 20
R/λ = 40
$\sigma^{\perp}(\theta)/\lambda^2$
10^6
10^5
10^4
10^3
10^2
10
0
10
20
30
θ (deg)

Fig. 9

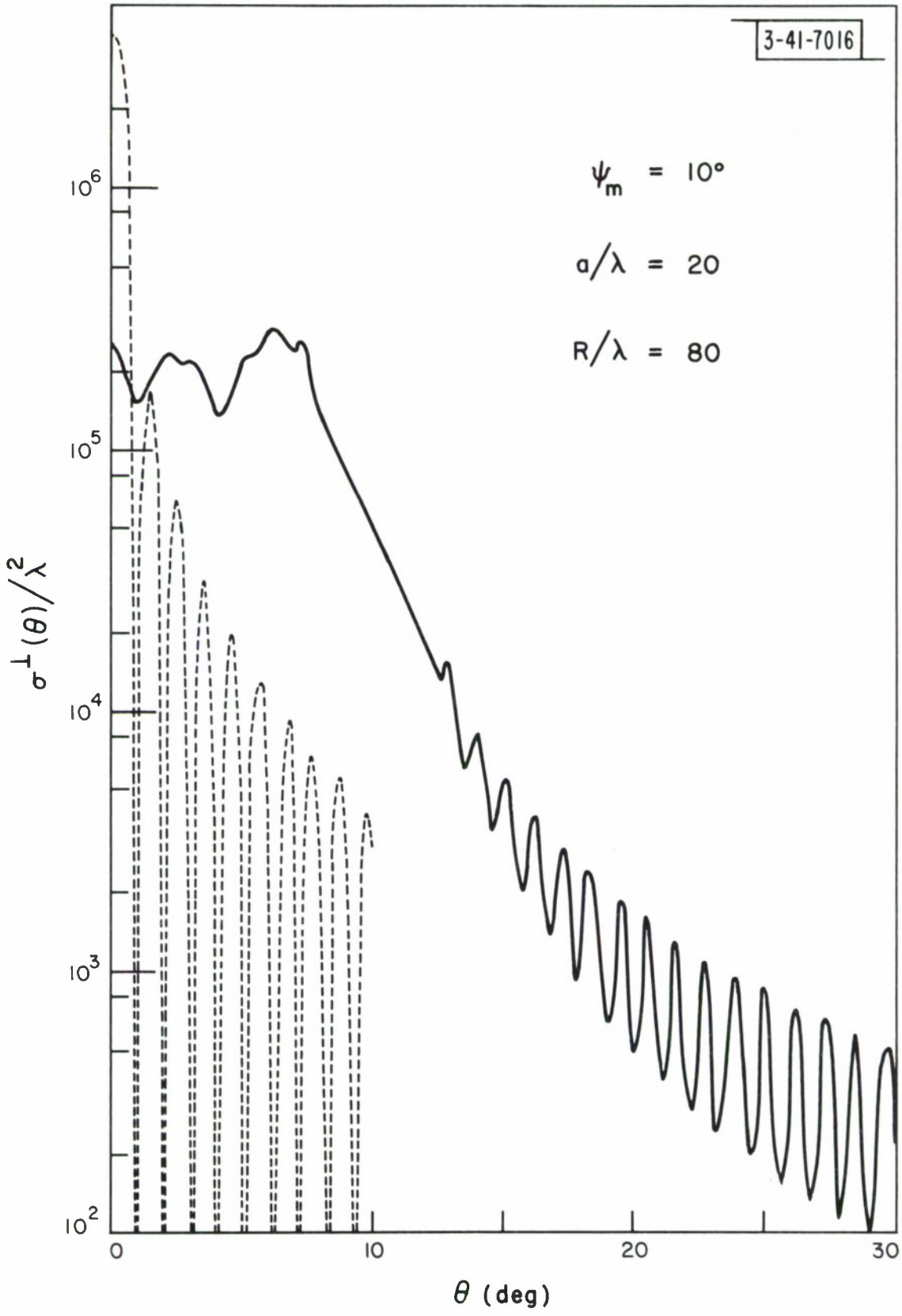
3-41-7016
ψ_m = 10°
a/λ = 20
R/λ = 80
10^6
10^5
10^4
10^3
10^2
$\sigma^{\perp}(\theta)/\lambda^2$
0
10
20
30
θ (deg)

Fig. 10

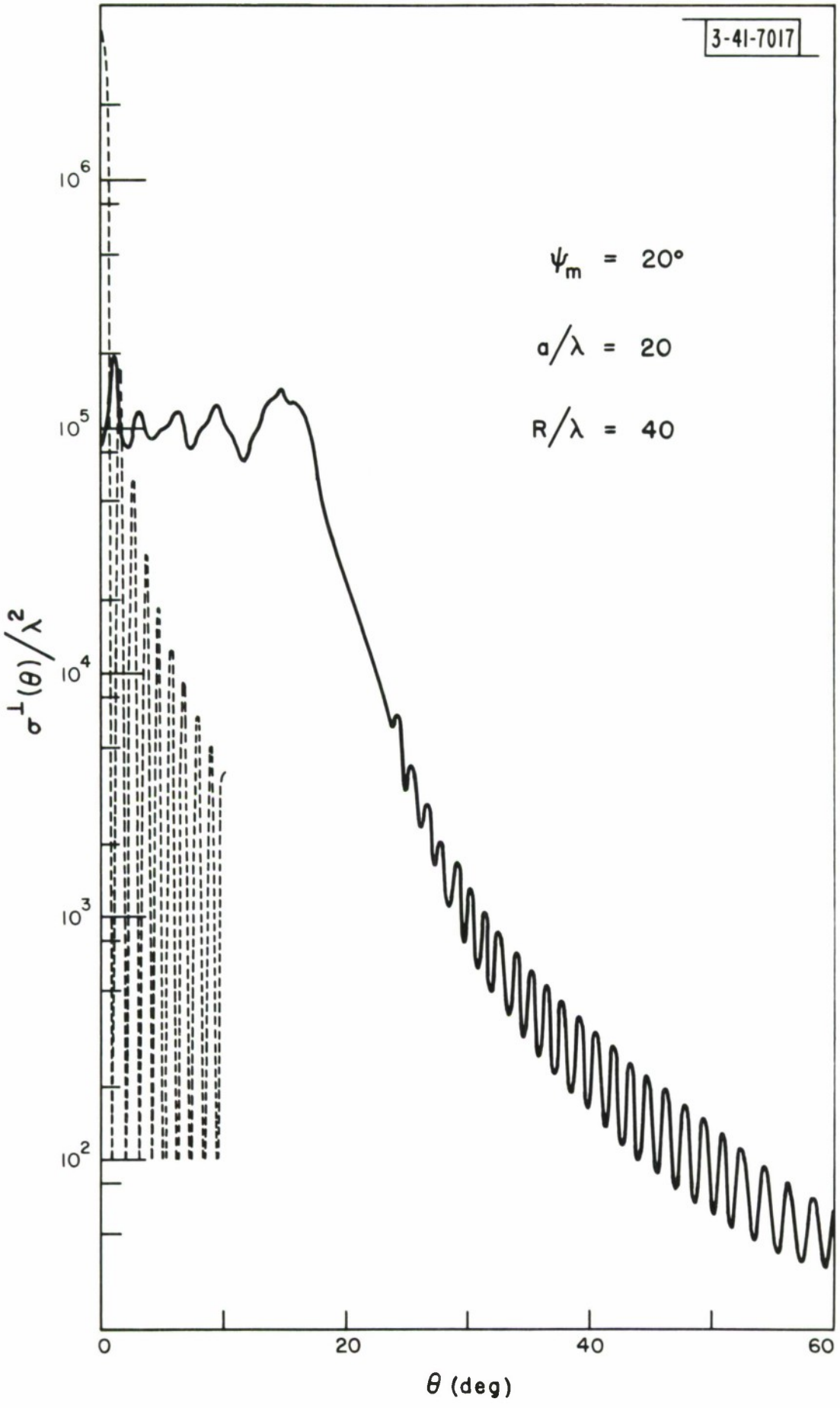
3-41-7017
ψ_m = 20°
a/λ = 20
R/λ = 40
$\sigma^{\perp}(\theta)/\lambda^2$
10^6
10^5
10^4
10^3
10^2
0
20
40
60
θ (deg)

Fig. 11

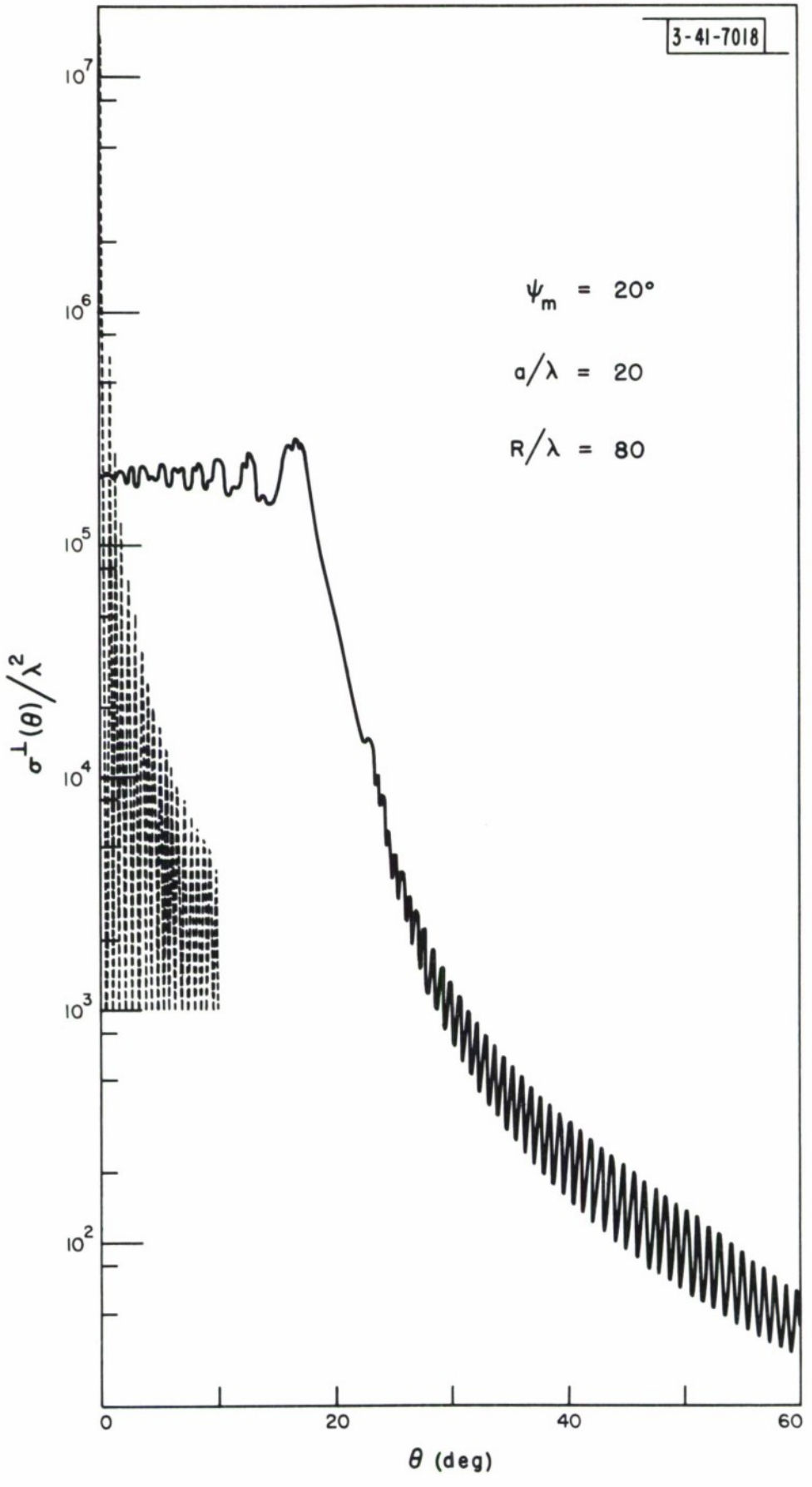
3-41-7018
ψ_m = 20°
a/λ = 20
R/λ = 80
$\sigma^{\perp}(\theta)/\lambda^2$
10^7
10^6
10^5
10^4
10^3
10^2
0
20
40
60
θ (deg)

Fig. 12

FIGURE CAPTIONS

1. Flat plate geometry

2a.
2b. Curved plate geometry (concave incidence)

3. Deformed integration contour

4a.
4b. Curved plate geometry (convex incidence)

5-8. Backscattering cross section from a circular cylindrical section for incidence in the longitudinal plane for four combinations of R/λ and ψ_m.

9-12. Backscattering cross sections from a circular cylindrical section (solid curve) and from the equivalent flat plate (dashed curve) for incidence in the transverse plane for four combinations of R/λ and ψ_m.

REFERENCES

1. See, for example, A. E. Puckett and S. Ramo, Guided Missile Engineering, (McGraw-Hill, 1959), p. 371.

2. P. M. Marcus, "Reflection of Radiation from Curved Surfaces," MIT Radiation Laboratory, Report 1029, (1946).

3. J. B. Keller, "Reflection and Transmission of Electromagnetic Waves by Thin Curved Shells," Journal of Applied Physics, 21, 896-901 (September, 1950).

4. J. B. Keller, "Diffraction by a Convex Cylinder," IRE Trans. on Ant. and Prop., AP-4, No. 3, 312-321 (July, 1956).

5. J. Steinberg, and B. Wolf, "Reflection of a Plane Wave by a Cylinder of Arbitrary Cross Section," RCA DAMP Tech. Monograph 62-04, (1962).

6. S. Silver, Microwave Antenna Theory and Design, (McGraw-Hill, 1959) Ch. 5 and pp. 180-182.

7. This is the method of stationary phase. For more details see, for example, A. Erdelyi, Asymptotic Expansions, (Dover, 1956).

DISTRIBUTION

Division 4

J. Freedman

Group 41

D. L. Clark (5)
M. Axelbank
S. L. Borison
W. F. Higgins
E. M. Hofstetter
H. M. Jones
J. J. G. McCue
J. B. Resnick
H. Schneider
C. B. Slade
E. B. Temple
D. M. Towle
R. E. VanderSchuur

Group 42

J. Margolin

Group 44

W. P. Delaney

Group 45

W. W. Ward
J. P. Perry
D. F. DeLong
M. W. Dill

Group 22

J. Rheinstein

M. I. T.

N. Durlach